Acta Oceanol. Sin., 2024, Vol. 43, No. 3, P. 127–138
https://doi.org/10.1007/s13131-023-2280-9
http://www.aosocean.com
E-mail: ocean2@hyxb.org.cn

An improved algorithm for retrieving thin sea ice thickness in the Arctic Ocean from SMOS and SMAP L-band radiometer data

Lian He[1, 2], Senwen Huang[1, 2], Fengming Hui[1, 2], Xiao Cheng[1, 2*]

[1] School of Geospatial Engineering and Science, Sun Yat-Sen University, and Southern Marine Science and Engineering Guangdong Laboratory (Zhuhai), Zhuhai 519082, China

[2] Key Laboratory of Comprehensive Observation of Polar Environment (Sun Yat-Sen University), Ministry of Education, Zhuhai 519082, China

Received 7 September 2023; accepted 27 November 2023

Abstract

The aim of this study was to develop an improved thin sea ice thickness (SIT) retrieval algorithm in the Arctic Ocean from the Soil Moisture Ocean Salinity and Soil Moisture Active Passive L-band radiometer data. This SIT retrieval algorithm was trained using the simulated SIT from the cumulative freezing degree days model during the freeze-up period over five carefully selected regions in the Beaufort, Chukchi, East Siberian, Laptev and Kara seas and utilized the microwave polarization ratio (PR) at incidence angle of 40°. The improvements of the proposed retrieval algorithm include the correction for the sea ice concentration impact, reliable reference SIT data over different representative regions of the Arctic Ocean and the utilization of microwave polarization ratio that is independent of ice temperature. The relationship between the SIT and PR was found to be almost stable across the five selected regions. The SIT retrievals were then compared to other two existing algorithms (i.e., UH_SIT from the University of Hamburg and UB_SIT from the University of Bremen) and validated against independent SIT data obtained from moored upward looking sonars (ULS) and airborne electromagnetic (EM) induction sensors. The results suggest that the proposed algorithm could achieve comparable accuracies to UH_SIT and UB_SIT with root mean square error (RMSE) being about 0.20 m when validating using ULS SIT data and outperformed the UH_SIT and UB_SIT with RMSE being about 0.21 m when validatng using EM SIT data. The proposed algorithm can be used for thin sea ice thickness (<1.0 m) estimation in the Arctic Ocean and requires less auxiliary data in the SIT retrieval procedure which makes its implementation more practical.

Key words: Arctic sea ice, sea ice thickness, remote sensing, Soil Moisture Active Passive (SMAP), Soil Moisture Ocean Salinity and Soil (SMOS)

Citation: He Lian, Huang Senwen, Hui Fengming, Cheng Xiao. 2024. An improved algorithm for retrieving thin sea ice thickness in the Arctic Ocean from SMOS and SMAP L-band radiometer data. Acta Oceanologica Sinica, 43(3): 127–138, doi: 10.1007/s13131-023-2280-9

1 Introduction

Arctic sea ice plays a significant role in the Earth's climate system. During the past few decades, sea ice across the Arctic Ocean shows a rapid decline in area, thickness, and age (Maslanik et al., 2011; Kwok, 2018; Liu et al., 2020) and thick multiyear ice is being replaced with thin, young ice (Meier et al., 2014), which highlights the importance of the monitoring of thin sea ice. The thickness of sea ice is an essential parameter that determines the energy and mass exchange between the atmosphere and the underlying ocean and thin sea ice with thickness less than 0.5 m dominates the surface heat budget (Maykut, 1978). Meanwhile, thinning sea ice is opening up the potential for increasing Arctic maritime traffic. Therefore, accurate knowledge of sea ice thickness (SIT) is crucial for weather and climate modelling as well as ship navigation.

A number of remote sensing tools are available to measure SIT. Satellite altimetry, including radar and laser altimetry, has been widely used for SIT estimation in the Arctic Ocean (Laxon et al., 2003; Kwok and Cunningham, 2008). However, the relative error of altimeter-based sea ice thickness measurements is large for thin sea ice (Laxon et al., 2003; Kaleschke et al., 2010; Ricker et al., 2017). Thermal infrared (TIR) imagery is capable of retrieving thin ice thickness with relatively high spatial resolution from the ice surface temperature based on the ice surface heat balance equation (Yu and Rothrock, 1996; Wang et al., 2010), but TIR data suffer from severe cloud contamination, leading to spatiotemporal discontinuities in the SIT products. Passive microwave (PMW) radiometer represents an important data source for retrieving thin ice thickness based on the dependence of ice emissivity on SIT (Martin et al., 2004; Iwamoto et al., 2013; Mäkynen and Similä, 2019) and could provide Arctic basin-wide measurements of thin ice thickness with daily temporal resolution and better accuracy for thin ice (Ricker et al., 2017).

High-frequency PMW radiometer data at frequencies of 19 GHz and 89 GHz have been used for Arctic thin ice thickness estimation, such as the Special Sensor Microwave Imager (SSM/I) (Cavalieri, 1994; Martin et al., 2004; Tamura and Ohshima, 2011), Advanced Microwave Scanning Radiometer-Earth

Foundation item: The National Natural Science Foundation of China under contract Nos 41830536 and 41925027; the Guangdong Natural Science Foundation under contract No. 2023A1515011235; the Innovation Group Project of Southern Marine Science and Engineering Guangdong Laboratory (Zhuhai) under contract No. 311021008.
*Corresponding author, E-mail: chengxiao9@mail.sysu.edu.cn

Observing System (AMSR-E) (Martin et al., 2005; Singh et al., 2011; Iwamoto et al., 2013; Scott et al., 2014; Kashiwase et al., 2019) and Advanced Microwave Scanning Radiometer 2 (AMSR2) (Yoshizawa et al., 2018; Mäkynen and Similä, 2019, 2022). Cavalieri (1994) found that the microwave polarization ratio (PR) at 19.4 GHz, i.e., PR(19), from SSM/I is sensitive to changes in ice thickness and ice surface characteristics and can be used to the map the distribution of new ($\leqslant$10 cm), young (11–30 cm) and first-year (30–80 cm) sea ice in the Arctic Ocean. Inspired by this study, retrieval algorithms have been proposed to quantitatively estimate SIT based on linear or exponential regression equations between SIT and microwave radiometer observations such as the polarization ratio, the spectral gradient ratio (GR), and the ratio between different brightness temperatures (R). These empirical sea ice retrieval algorithms utilize high frequencies which rely on the assumption that thin ice emission depends mainly on near surface salinity that decreases with increasing SIT (Naoki et al., 2008; Mäkynen and Similä, 2019). Their maximum retrievable ice thickness is about 10 cm to 20 cm (Martin et al., 2004; Tamura and Ohshima, 2011). Meanwhile, attempts have been made to retrieve thick ice thickness from the high-frequency radiometer data based on the empirical relationship between microwave radiometer observations and ice freeboards (Lee et al., 2021; Kim et al., 2022) or ice thickness (Kim et al., 2020; Chi and Kim, 2021; Soriot et al., 2023).

The Soil Moisture and Ocean Salinity (SMOS) mission of the European Space Agency (ESA) and the Soil Moisture Active Passive (SMAP) satellite of the National Aeronautics and Space Administration (NASA) provide global observations of L-band (1.4 GHz) passive microwave brightness temperature (TB) observations at a resolution of about 40 km. The L-band brightness temperature of sea ice mainly depends on its thickness, temperature and salinity (Menashi et al., 1993; Kaleschke et al., 2010), and can be used to retrieve SIT due to the high penetration depth as well as large brightness temperature contrast between ice and water at L band (Kaleschke et al., 2010, 2012). Tian-Kunze et al. (2014) proposed an iterative SIT retrieval algorithm based on a thermodynamic sea ice model and a three-layer radiative transfer model. This algorithm has been used for operational SMOS SIT product using the brightness temperature intensity averaged over incidence angles between 0° and 40° by the University of Hamburg (referred to as UH_SIT) and explicitly accounts for variations of ice temperature and ice salinity. However, the UH_SIT algorithm requires additional parameters such as air temperature and ice salinity, which introduces external errors to the SIT retrievals. Huntemann et al. (2014) developed an empirical SIT retrieval algorithm based on the SMOS brightness temperature intensity (I) and polarization difference (Q) averaged over incidence angles between 40° and 50°. This retrieval algorithm was further transferred from SMOS to SMAP by Paţilea et al. (2019) and was used to generated an operational SIT product by the University of Bremen (referred to as UB_SIT). Gupta et al. (2019) developed an empirical SIT retrieval model (referred to as BEC_SIT) which was trained using only airborne SIT data to estimate SIT from SMOS polarization difference at 50°. Some of these algorithms have been evaluated using reanalysis data (Tietsche et al., 2018) or upward looking sonar data (Sánchez-Gámez et al., 2020). All the above algorithms rely on the brightness temperature for SIT retrieval. While the UH_SIT algorithm could account for the influence of ice temperature but requires more additional parameters for SIT retrieval, the UB_SIT and BEC_SIT algorithms could not correct the ice temperature influence.

The objective of this study was to develop an improved thin ice thickness retrieval algorithm for the SMAP and SMOS L-band radiometer data. Simulated SIT data obtained from the cumulative freezing degree days (CFDD) model (Bilello, 1961) during the freeze-up period over five regions in Beaufort, Chukchi, East Siberian, Laptev and Kara seas were used as reference data to train an empirical SIT retrieval algorithm using the polarization ratio of SMAP and SMOS data. The utilization of PR helps to minimize the influence of the physical ice temperature since it is a ratio of observed brightness temperatures. The newly proposed algorithm was then evaluated through comparisons with other two existing SIT products (UH_SIT and UB_SIT) and validations against *in situ* SIT measurements collected by moored upward looking sonars (ULSs) and airborne electromagnetic (EM) induction sensors, respectively.

2 Study area and data

2.1 *Study area*

Figure 1 displays the study area of this study. The Arctic region is divided into 10 sub-regions, including Beaufort Sea, Chukchi Sea, East Siberian Sea, Laptev Sea, Kara Sea, Barents Sea, Central Artic Ocean, Greenland Sea, Baffin Bay and Canadian Archipelago. Five areas marked by green rectangles with a size of 125 km by 125 km are carefully selected to obtain reference data of SIT based on the CFDD model (Bilello, 1961). The black dots in the Beaufort Sea and the Laptev Sea represent the locations where SIT measurements were obtained from moored upward looking sonars. The black stars indicate the locations where field campaigns were conducted to measure SIT using an airborne EM induction sensor.

2.2 *Study data*

2.2.1 *SMOS brightness temperature data*

The SMOS mission was designated for global observations of soil moisture over land and salinity over oceans (Kerr et al., 2001). The SMOS satellite was launched in November 2009, and it carries the Microwave Imaging Radiometer using Aperture Synthesis (MIRAS) instrument. MIRAS is a passive microwave 2-D interferometric radiometer and could acquire L-band (1.4 GHz) brightness temperature measurements in full polarization mode at a range of incidence angles from 0° to about 70° with a spatial resolution of 35 km to 50 km.

In this study, the SMOS Level 1C (L1C) brightness temperature product (Version 724) was used, which is geolocated in an equal-area grid system of ISEA 4H9 (Icosahedral Snyder Equal Area projection with aperture 4, resolution 9) with a spatial resolution of 15 km. The SMOS L1C data were reprojected to the 25-km NSIDC polar stereographic north projection using the average resampling method. For each 25 km grid, the daily mean was calculated by averaging the observations within the incidence angle range of 38.5° and 41.5°. In order to remove outliers, measurements that deviate from the mean values by more than two standard deviations were discarded in calculating the daily mean for each grid.

2.2.2 *SMAP brightness temperature data*

The SMAP mission was designed for the measurement of soil moisture and freeze/thaw state to better understand water, carbon and energy cycles (Entekhabi et al., 2010). The SMAP satellite was launched in January 2015, and it consists of L-band radar and radiometer sensors for simultaneous active and passive mi-

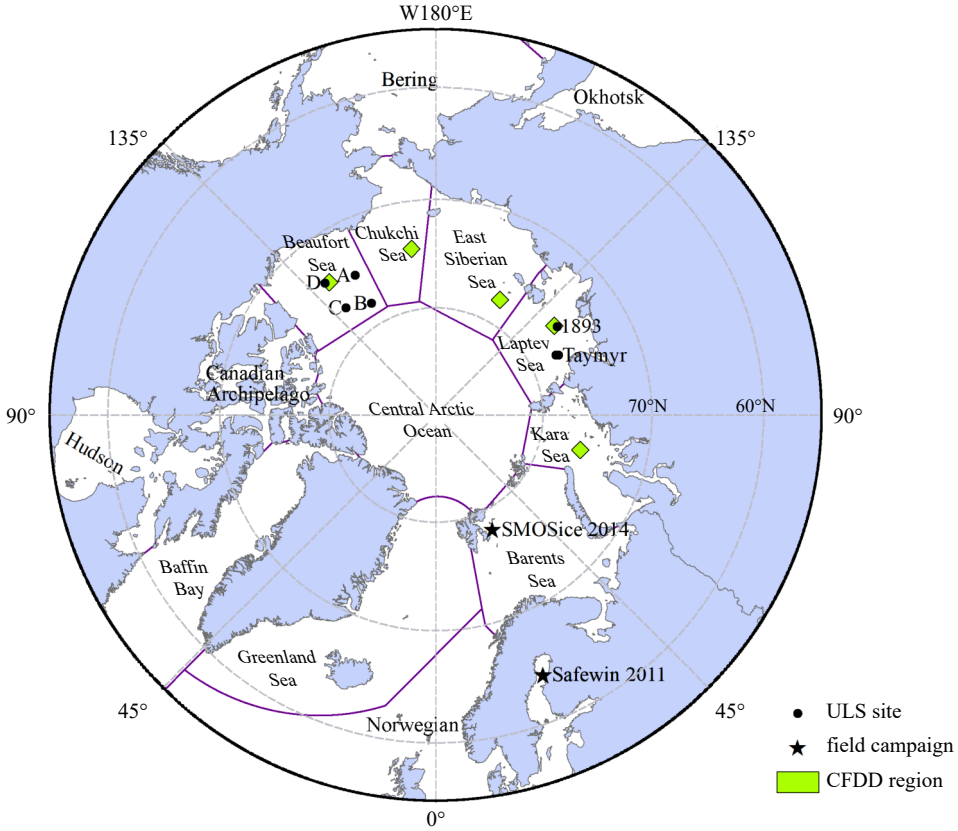

Fig. 1. Study area and data locations in the Arctic. Black dots indicate the locations of moored upward looking sonars (ULSs) in the Beaufort Sea (i.e., A, B, C and D) and in the Laptev Sea (i.e., 1893 and Taymyr). Black stars represent the locations of field campaigns (i.e., SMOSice 2014 and Safewin 2011). Green rectangles indicate the areas selected to simulate sea ice thickness using the cumulative freezing degree days (CFDD) model.

crowave data acquisition with a fixed incidence angle of approximately 40°. The radiometer could provide L-band (1.4 GHz) brightness temperature observations at spatial resolution of about 40 km. Compared to SMOS, SMAP has adopted radio frequency interference (RFI) detection and mitigation measures to reduce the effects of RFI.

The SMAP enhanced L1C radiometer brightness temperature product (SPL1CTB_E, Version 3) (Chaubell et al., 2020) utilized in this study, which is derived from SMAP Level-1B (L1B) interpolated antenna temperatures using the Backus-Gilbert interpolation technique (Backus and Gilbert, 1967). The SPL1CTB_E product contains calibrated and geolocated brightness temperatures that are gridded using an Earth-fixed, global cylindrical 9 km Equal-Area Scalable Earth Grid, Version 2.0 (EASE-Grid 2.0) projection for both descending and ascending orbits. The daily brightness temperature data were obtained by averaging the ascending and descending data and were then reprojected to the 25-km NSIDC polar stereographic north projection using the average resampling method.

2.2.3 *Moored ULS data*

In situ SIT measurements obtained from ULSs deployed in the Beaufort Sea and Laptev Sea were collected to validate SIT estimates. The first SIT dataset was obtained from the Beaufort Gyre Exploration Project (BGEP), which was established in 2003 and aims to measure the content and fluxes of freshwater and heat in the Beaufort Gyre (BG) using a number of moorings. These moorings were deployed in the Beaufort Sea and could provide time series measurements of temperature, salinity, currents, sea ice draft and bottom pressure. Sea ice draft observations at three mooring locations (A, B and D) (Krishfield et al., 2014) during 2010 and 2021 were used. Another SIT dataset was obtained from an ULS in the Laptev Sea from September 2013 to August 2015 at the Taymyr and 1893 stations (Belter et al., 2019). The spatial distribution of the moorings is indicated by black dots in Fig. 1.

ULS could measure sea ice draft with an accuracy of ±5 cm in most cases (Krishfield and Proshutinsky, 2006). Sea ice thickness could be estimated by multiplying the sea ice draft with a factor of 1.09 without considering the ice types and snow thickness (Fukamachi et al., 2017). In order to compare daily ULS data to satellite SIT retrievals, hourly ULS data were averaged to daily mean values.

2.2.4 *EM sea ice thickness data*

EM induction measurements of SIT from two campaigns were collected to assess the accuracy of SIT retrievals, including SafeWin 2011 (Haas et al., 2021) and SMOSice 2014 (Hendricks et al., 2014; Kaleschke et al., 2016), which have been indicated in Fig. 1. All SIT data were acquired in springtime using the electromagnetic induction system, which utilizes the contrast of electrical conductivity between sea water and sea ice to determine its distance to the ice-water interface. The accuracy of the EM measurements is in the order of ±10 cm over level sea ice (Pfaffling et al., 2007). However, the accuracy could be worse over ridged ice due to the diffusivity of the low-frequency EM field (Reid et al., 2006).

The SafeWin 2011 field campaign was carried out in the

northern Baltic Sea in March 2011. A total of 11 flights were performed and covered large parts of the Sea and Bay of Bothnia. The SMOSice 2014 campaign was conducted on newly formed thin sea ice regions in the Barents Sea south-east of the Svalbard in March 2014 and has collected a comprehensive data set of high resolution L-band radiometer data, auxiliary sea ice conditions and SIT data in support of the development and improvement of the SMOS SIT retrieval algorithm (Hendricks et al., 2014; Kaleschke et al., 2016). All the airborne EM SIT data were reprojected to the 25-km NSIDC polar stereographic north projection using the average resampling method to align with the satellite radiometer data.

2.2.5 *Sea ice concentration data*

The sea ice concentration (SIC) data produced by the Integrated Climate Data Center (ICDC), University of Hamburg are collected. The SIC data are derived from the ARTIST Sea Ice (ASI) algorithm to brightness temperatures measured with the 85 GHz SSM/I and Special Sensor Microwave Imager/Sounder (SSMI/S) channels (Kaleschke et al., 2001; Spreen et al., 2008). This product has been provided on a polar-stereographic grid true at 70° with 12.5 km grid resolution since December 1991 and was reprojected to the 25-km NSIDC polar stereographic north projection using the average resampling method. This SIC product was utilized to identify the presence of sea ice in the CFDD model and to correct the effects of open water.

3 Methods

3.1 *CFDD sea ice growth model*

In order to train a SIT retrieval algorithm, reference data were required. Due to the lack of *in situ* SIT measurements in polar regions especially in thin ice areas, simulated sea ice thickness data during the freeze-up period from the CFDD sea ice growth model (Bilello, 1961) were used as reference data. Previous results have indicated that despite the simplicity of the CFDD model, its predicted SIT values correlate very well with the ULS *in situ* data during the sea ice growth season (Sánchez-Gámez et al., 2020). Therefore, this study utilized the CFDD simulated SIT data to train the retrieval algorithm. The sea ice thickness can be related to the CFDD as follows (Bilello, 1961):

$$\mathrm{SIT} = 1.33 \times \mathrm{CFDD}^{0.58}, \tag{1}$$

where SIT is the sea ice thickness in centimeter and CFDD is calculated by integrating over the time when the first sea ice is present as

$$\mathrm{CFDD} = \int_0^t (T_\mathrm{f} - T_\mathrm{a})\,\mathrm{d}t, \tag{2}$$

where T_a is the daily average air temperature in degree Celsius (℃), T_f is the freezing point of sea water (–1.8℃), and $T_\mathrm{a} < T_\mathrm{f}$. The daily 2 m air temperature data produced by the National Center for Environmental Prediction (NCEP) and the National Center for Atmospheric Research (NCAR) (Kalnay et al., 1996) were used as the input in the CFDD model and can be available at https://psl.noaa.gov.

3.2 *Existing thin sea ice thickness retrieval algorithms*

A number of algorithms have been developed for retrieving SIT from SMOS radiometer data (Kaleschke et al., 2010, 2012; Huntemann et al., 2014; Tian-Kunze et al., 2014; Gupta et al., 2019). The algorithms developed at the University of Hamburg (UH) (Tian-Kunze et al., 2014) and the University of Bremen (UB) (Huntemann et al., 2014) have been used to generate operational thin ice thickness products of the Arctic which are available to the public. Therefore, these two algorithms were used for comparison in this study.

The SIT retrieval algorithm developed at the University of Hamburg (referred to UH_SIT) (Tian-Kunze et al., 2014) is based on a forward model that consists of a thermodynamic sea ice model and a three-layer radiative transfer model. The forward model is used to simulate brightness temperature and can account for variations of ice temperature and ice salinity. The sea ice thickness is iteratively solved by minimizing the difference of simulated and measured brightness temperatures. The UH_SIT algorithm further accounts for the statistical thickness distribution within one satellite pixel and can retrieve SIT up to 1.5 m. More details about this SIT retrieval algorithm can be found in Tian-Kunze et al. (2014).

The SIT retrieval algorithm developed at the University of Bremen (referred to as UB_SIT) is based on the empirical relationship between SIT and brightness temperature intensity I as well as polarization difference Q at incidence angles between 40° and 50°. I and Q can be expressed as a function of sea ice thickness as follows (Huntemann et al., 2014):

$$I_{abc}(x) = a - (a-b)\cdot\exp(-x/c), \tag{3}$$

$$Q_{abcd}(x) = (a-b)\cdot\exp\left[-(x/c)^d\right] + b, \tag{4}$$

where x is the sea ice thickness; a, b, c and d are parameters to be determined from the regression of sea ice thickness data on microwave data.

In the UB_SIT algorithm, SIT data simulated using a CFDD ice growth model in the Kara and Barents seas were used as reference to obtain the parameters of a, b, c and d. The maximum retrievable SIT reaches up to 0.5 m. In addition, the UB_SIT algorithm only uses brightness temperatures in SIT estimation and does not correct the effect of open water. Therefore, it is only applicable to the case of high sea ice concentration. Meanwhile, only two regions (the Kara and Barents seas) were selected to train the retrieval algorithm, which may not be representative of all possible conditions since the ice salinity varies from region to region and the ice temperature varies from time to time.

3.3 *Improved thin sea ice thickness retrieval algorithm*

Previous studies have demonstrated that microwave radiometer observations such as the polarization ratio, the spectral gradient ratio, and the ratio between different brightness temperatures are sensitive to SIT and can be used for SIT retrieval (Martin et al., 2004, 2005; Singh et al., 2011; Tamura and Ohshima, 2011; Iwamoto et al., 2013; Scott et al., 2014; Mäkynen and Similä, 2019, 2022). This study employed the PR of microwave brightness temperature to retrieve SIT, which is defined as

$$\mathrm{PR}(f) = \frac{\mathrm{TB_V}(f) - \mathrm{TB_H}(f) - k_1(1-C)}{\mathrm{TB_V}(f) + \mathrm{TB_H}(f) - k_2(1-C)}, \tag{5}$$

where PR(f) indicates the polarization ratio at frequency f; $\mathrm{TB}_p(f)$ is the brightness temperature at p polarization (i.e., V or H) and frequency f; C is the sea ice concentration; k_1 and k_2 are correc-

tion terms for the contribution of open water when sea ice concentration is below 100% and can be written as follows:

$$k_1 = \mathrm{TB}_{\mathrm{V}}^{\mathrm{OW}}(f) - \mathrm{TB}_{\mathrm{H}}^{\mathrm{OW}}(f), \tag{6}$$

$$k_2 = \mathrm{TB}_{\mathrm{V}}^{\mathrm{OW}}(f) + \mathrm{TB}_{\mathrm{H}}^{\mathrm{OW}}(f), \tag{7}$$

where $\mathrm{TB}_p^{\mathrm{OW}}(f)$ indicates brightness temperature at frequency f with polarization p (V or H) over open water. For SMAP data, the open water tie-points were set as 115.90 K and 76.91 K for horizontal and vertical polarization, respectively, which were empirically determined using the method in Ivanova et al. (2015) .

The advantage of PR is that it is largely independent of the physical ice temperature since it is a ratio of observed brightness temperatures. After the calculation of PR(1.4) from SMOS and SMAP, an exponential equation was utilized to describe the dependence of PR(1.4) on SIT as follows (Martin et al., 2004; Iwamoto et al., 2013):

$$\mathrm{SIT} = \exp\left(\frac{1}{\alpha \cdot \mathrm{PR} + \beta}\right) - \gamma, \tag{8}$$

where SIT is the sea ice thickness (m); α, β and γ are parameters to be determined from the exponential regression of CFDD SIT data on microwave PR data. The curve is fitted using the total least square method (Petráš and Bednárová, 2010).

4 Results and discussion

4.1 *Relationship between PR(1.4) and sea ice thickness*

In order to investigate the relationship between polarization ratio PR(1.4) and sea ice thickness, the three-layer (water-ice-air) dielectric slab model (Menashi et al., 1993; Kaleschke et al., 2010) was utilized to simulate sea ice emissivities under different conditions. In this model, the sea ice is considered as a homogeneous medium over sea water and characterized by dielectric constant and thickness. The input parameters include sea ice thickness, sea ice salinity (S_{ice}, related to ice dielectric constant) and sea ice thickness variation (σ_{d}). Figure 2 displays the changes of PR(1.4) as a function of SIT, S_{ice} and σ_{d}, which confirms that the exponential equation in Eq. (8) can be utilized to describe the dependence of PR(1.4) on SIT. It can also be observed that PR(1.4) is most sensitive to ice thickness among the three input parameters, inferring that PR(1.4) can be used for ice thickness estimation.

The relationship between the CFDD sea ice thicknesses and the SMOS and SMAP PR(1.4) values was then examined over five selected regions (5 × 5 grids with 25 km intervals in the Beaufort, Chukchi, East Siberian, Laptev, and Kara seas as indicated in Fig. 1). These five areas are carefully selected according to the time series of their sea ice concentration, ice drift speed and air temperature data. The mean sea ice drift speeds of these five areas range from 9.1 km/day in the Laptev Sea to 13.1 km/day in the Kara Sea according to the Ocean and Sea Ice Satellite Application Facility (OSI-SAF) sea ice drift product (OSI-405-c) (Lavergne et al., 2010). The ice drift speeds are of the order of a half of the size of the 25 km grid cell. Therefore, the CFDD model is applicable without introducing larger errors according to Huntemann et al. (2014). In order to further reduce the accumulated error of the CFDD model, only SIT data within 75 days after the first appearance of sea ice were used.

Figure 3 displays the density scatter plots of sea ice thicknesses against SMOS and SMAP PR(1.4) values from the 5 selected regions. It can be observed that PR(1.4) shows a monotonic decrease for increasing ice thickness, which allows for the retrieval of SIT from the measured polarization ratio. The sensitivity of PR(1.4) to SIT decreases with increasing SIT. A significant level of sensitivity can be detected when the ice thickness is below 0.5 m. However, the sensitivity is considerably reduced when the sea ice thickness is above 0.5 m. These results agrees well with the results of Kaleschke et al. (2010). The exponential equation was utilized to fit the relationship between PR(1.4) and SIT. SMAP exhibits a higher training accuracy compared to SMOS, with their root mean square error (RMSE) values being 0.12 m and 0.14 m, respectively. This difference may be due to the fact that the radiometric uncertainty of SMAP is higher than that of SMOS.

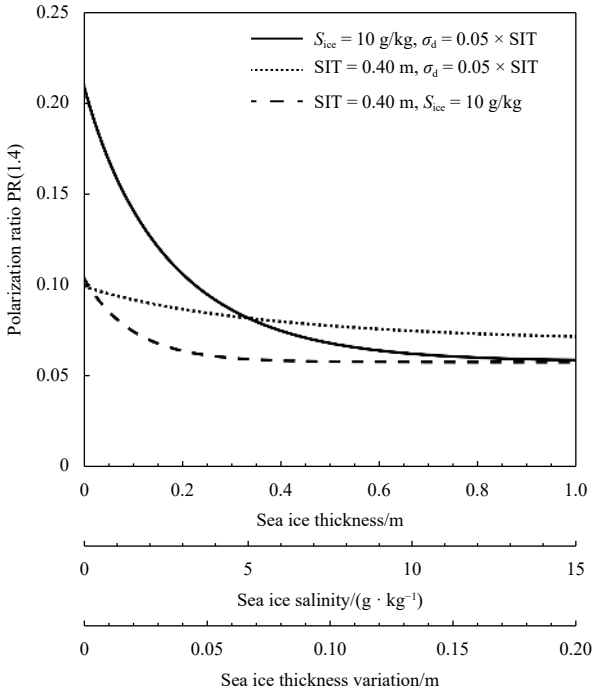

Fig. 2. Change of polarization ratio PR(1.4) as a function of sea ice thickness (SIT), sea ice salinity (S_{ice}) and sea ice thickness variation (σ_{d}) simulated using the three-layer sea ice emissivity model (Menashi et al., 1993; Kaleschke et al., 2010). In each case two parameters have been kept constant while the third parameter was varied.

4.2 *Variability of regression coefficients*

In order to study the variability of the regression coefficients of Eq. (8), the regression is performed for each region. Figure 4 displays the fitting curves for the five selected regions and Table 1 summarizes the regression coefficients separately trained on these five regions. Results using all regions' data are also included. For both SMOS and SMAP, the fitting curves are close to each other except that the Beaufort Sea deviates from the other seas. The curve for the Beaufort Sea tends to underestimate the sea ice thickness by a maximum value of about 0.05 m for PR(1.4) between 0.05 and 0.15. The maximum difference among the predicated values from different models is within 0.1 m when the PR(1.4) is greater than 0.05. These results indicate that the relationship between SIT and PR(1.4) is almost stable across different regions in the Arctic. It should be noted that the ice salinity and ice temperature may vary from region to region and the selection of these five regions may be representative of all possible

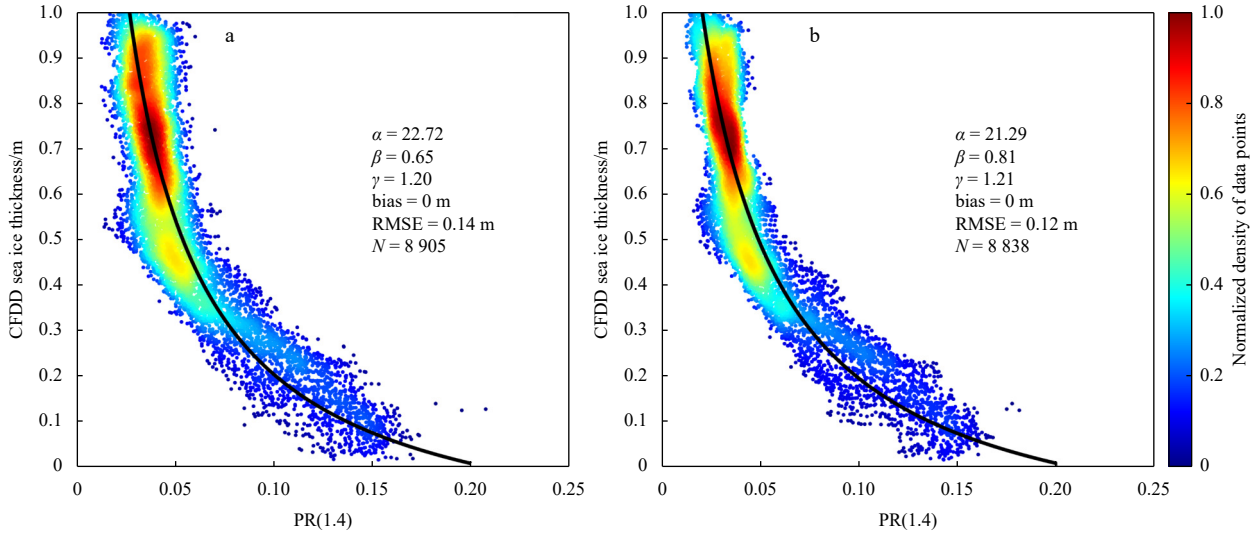

Fig. 3. Density scatterplots of cumulative freezing degree days (CFDD) model sea ice thickness and PR(1.4) for SMOS (a) and SMAP (b), respectively. RMSE, root mean square error; *N*, number of available measurements.

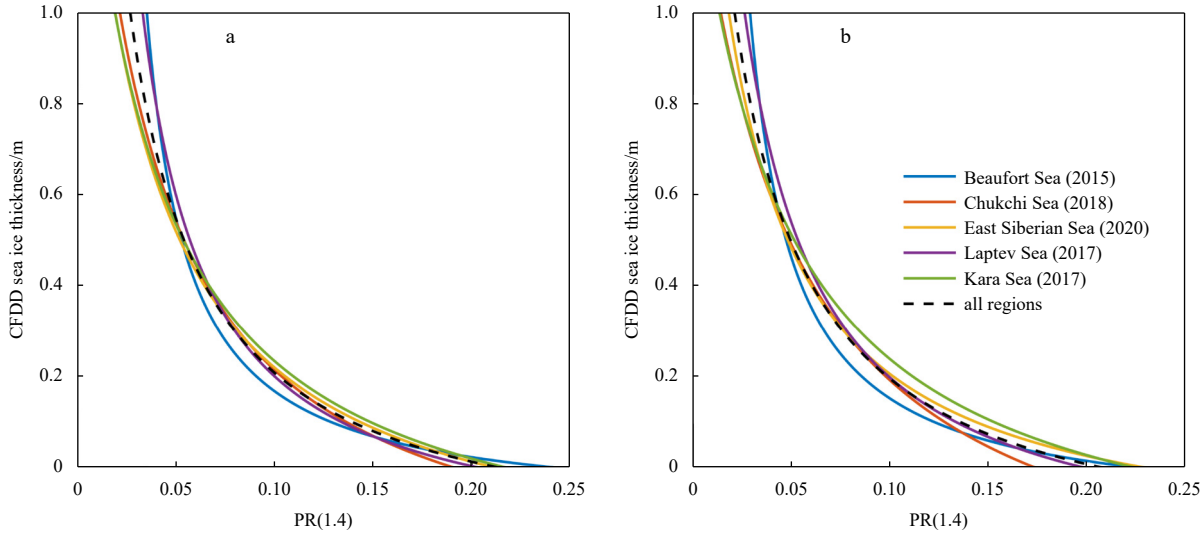

Fig. 4. Fitting curves for the selected areas in this study for SMOS (a) and SMAP (b).

Table 1. Regression coefficients (α, β and γ) and number of available measurements (N) over the five selected areas for SMOS and SMAP

Region (year)	Regression coefficients and number of available measurement							
	SMOS				SMAP			
	α	β	γ	N	α	β	γ	N
Beaufort Sea (2015)	44.57	–0.24	1.10	1 839	41.66	0.13	1.11	1 766
Chukchi Sea (2018)	15.50	0.86	1.30	1 582	12.63	0.98	1.37	1 582
East Siberian Sea (2020)	16.98	0.90	1.25	1 830	21.10	0.89	1.19	1 830
Laptev Sea (2017)	26.44	0.39	1.19	1 810	21.85	0.68	1.22	1 810
Kara Sea (2017)	15.72	0.92	1.26	1 844	14.03	1.03	1.27	1 850
	22.72	**0.65**	**1.20**	**8 905**	**21.29**	**0.81**	**1.21**	**8 838**

Note: Bold values are for all regions.

conditions. Therefore, the models for SMOS and SMAP should be applicable to the entire Arctic Ocean.

4.3 *Comparison of thin sea ice thickness retrievals*

Four Arctic thin SIT products are compared, including SMOS_SIT, SMAP_SIT, UH_SIT and UB_SIT. As a demonstration, Fig. 5 displays the spatial distributions of these four products on November 15, 2019. It can be seen that SMOS_SIT shows a very similar spatial distribution of SIT to SMAP_SIT with a correlation value of about 0.92. The mean bias between these two data is within 0.01 m, indicating that the difference between SMOS_SIT and SMAP_SIT is minimal. Both SMOS_SIT and SMAP_SIT tend

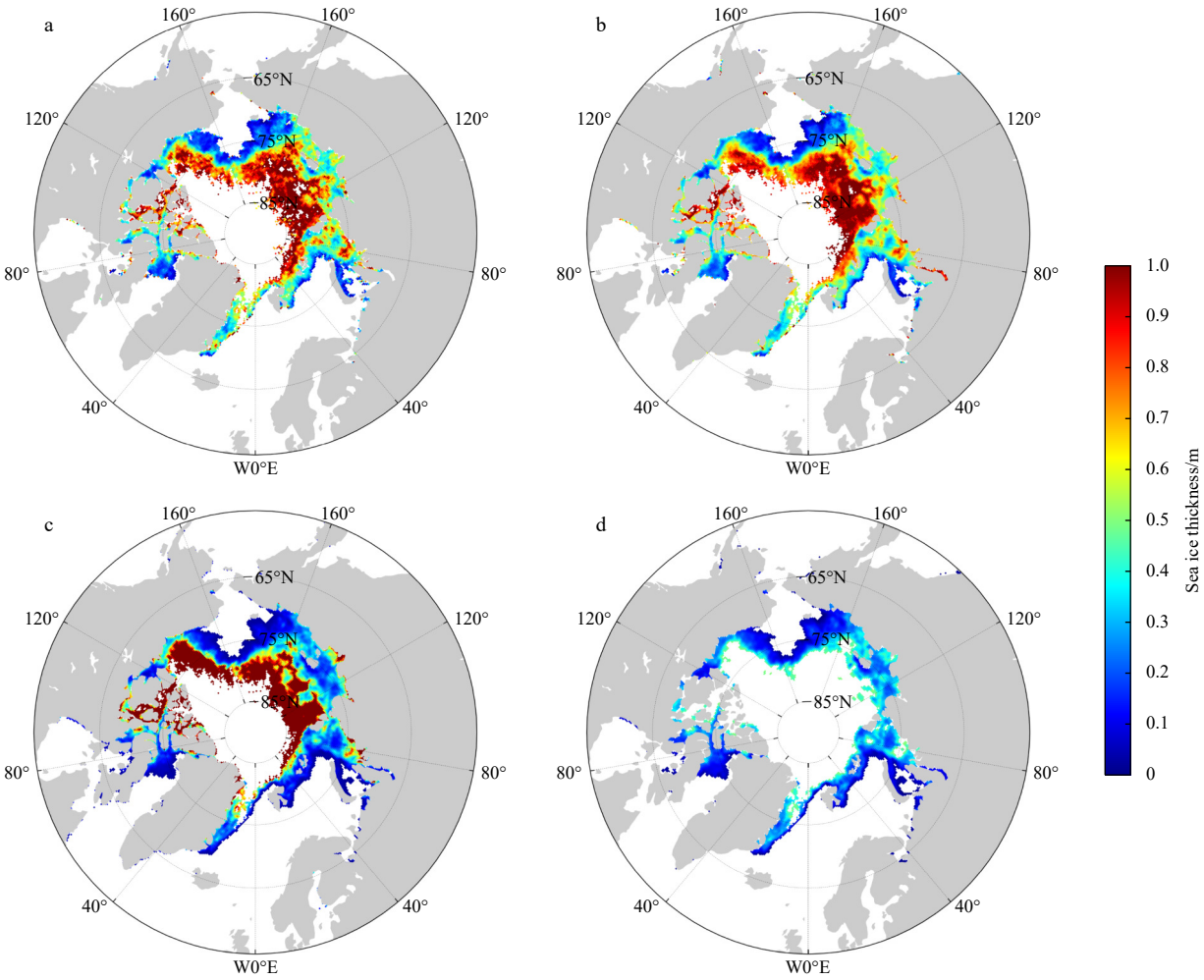

Fig. 5. Spatial distributions of Arctic thin sea ice thickness on November 15, 2019 from SMOS_SIT (a), SMAP_SIT (b), UH_SIT (c), and UB_SIT (d), respectively.

to yield higher SIT values in the marginal ice zone compared to UH_SIT and UB_SIT with mean bias values being 0.16 m and 0.17 m, respectively. This can be explained by that sea ice thicknesses from UH_SIT and UB_SIT are retrieved from brightness temperatures and the contribution of open water to the total brightness temperature is neglected in the retrieval algorithms, which leads to underestimation of SIT. By contrast, correction terms for the contribution of open water are applied for SMOS_SIT and SMAP_SIT when the sea ice concentration is below 100%. UH_SIT has the highest SIT values in the Central Arctic region and the Canadian Arctic Archipelago, where the retrieved SIT can reach up to 1.5 m. However, the maximal retrievable ice thickness of SMOS_SIT and SMAP_SIT is around 1.0 m in these areas. The ice thickness retrievals from SMOS_SIT and SMAP_SIT are lower than from UH_SIT, which may be explained by that the UH_SIT retrieval algorithm considers the SIT distribution within a satellite pixel to correct the underestimation of ice thickness caused by the plane ice layer assumption (Tian-Kunze et al., 2014; Kaleschke et al., 2016). Furthermore, the presence of snow on sea ice could change the overall brightness temperature of sea ice due to the insulation effect and the radiative contribution of the snow. The SMOS_SIT and SMAP_SIT algorithms are expected to be less affected by the insulation effect since the polarization ratio is independent of the physical ice temperature. However, the radiative contribution of the snow was ignored in this study since the snow cover is assumed to be transparent at L-band under dry conditions, which warrants further analysis.

4.4 *Assessment of uncertainties in the retrieved sea ice thickness*

The sea ice thickness was retrieved from the microwave polarization ratio at 1.4 GH, which relies on the TB measurements and SIC estimates. In order to analyze the uncertainties in SIT introduced by the input parameters of TB and SIC, a Monte Carlo approach was used. The Monte Carlo approach involves randomly varying the input parameters based on their respective probability distribution functions and running the retrieval algorithm multiple times to obtain a distribution of SIT values. The standard deviation of this distribution is used as a measure of the uncertainty in the retrieved SIT. In this study, the retrieval algorithm was run for 1 000 times for each pixel.

The SIT uncertainty from TB and SIC was evaluated separately. The uncertainty coming from brightness temperature is firstly calculated assuming that the sea ice concentration is accurately estimated. As an example, Fig. 6 shows the scatterplots of SIT retrievals and their respective uncertainties on November 15, 2019 for SMOS and SMAP, respectively. The radiometric uncertainties of brightness temperature for SMOS and SMAP were set as 2.5 K (McMullan et al., 2008; Corbella et al., 2011) and 1.3 K (Piepmeier et al., 2017; Peng et al., 2019), respectively. For both SMOS and SMAP, the uncertainties increase with increasing SIT,

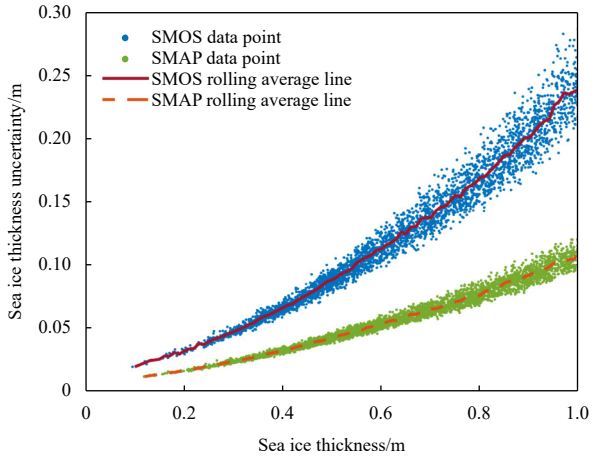

Fig. 6. Scatterplots of sea ice thickness retrievals and their respective uncertainties on November 15, 2019 in the Arctic for SMOS and SMAP, respectively. The lines show the rolling average of the uncertainty.

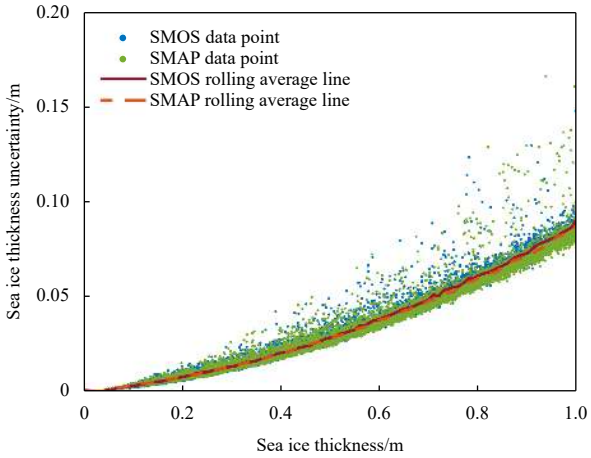

Fig. 7. Scatterplots of sea ice thickness retrievals and their respective uncertainties for a sea ice concentration uncertainty of 5% on November 15, 2019 in the Arctic for SMOS and SMAP, respectively. The lines show the rolling average of the uncertainty.

which is consistent with the results of Paţilea et al. (2019). The SMOS uncertainty is larger than that for SMAP since the uncertainty in SMOS TB measurements is larger than that for SMAP.

The uncertainty coming from SIC was then calculated by varying the SIC taking into account with ±5% standard deviation (Ivanova et al., 2015). Figure 7 displays the SIT uncertainty for SMOS and SMAP on November 15, 2019. Both SMOS and SMAP show a gradual increase in SIT error with increasing SIT, and they have similar levels of uncertainty. The uncertainty in ice thickness is close to zero at an ice thickness of 0 m and could reach approximately to 0.10 m at an ice thickness of 1.0 m. Moreover, the SIT uncertainty introduced by sea ice concentration is lower than that of brightness temperature.

4.5 *Validation of thin ice thickness retrievals*

4.5.1 *Validation using ULS sea ice thickness measurements*

Four SIT products (SMOS_SIT, SMAP_SIT, UH_SIT and UB_SIT) were validated against independent ice draft and thickness measurements obtained by upward looking sonar moorings deployed in the Beaufort Sea and Laptev Sea (Fig. 1). The maximum retrievable SIT is limited to 1.0 m for SMOS_SIT, SMAP_SIT and UH_SIT, while UB_SIT has maximum retrievable ice thickness of about 0.5 m. ULS ice thickness data from three BGEP ULS moorings (A, B and D) during the freezing period (October to January) from 2010 to 2021 and from two ULS moorings (Taymyr and 1893) during the freezing period (October to January) from 2013 to 2015 were utilized. Only ULS ice thickness measurements below 1.0 m were used to evaluate the ice thickness retrievals. Figure 8 displays the scatterplots between ULS SIT measurements and four SIT estimates. Since the SMAP radiometer data only dates back to March 2015, the validation result in the Laptev Sea for SMAP_SIT is not available.

The four ice thickness products show generally good consistency with ULS measurements with RMSE values being about 0.21 m and correlation coefficients (r) ranging from 0.59 to 0.66. There is no significant difference in retrieval accuracy among these four products in terms of RMSE and r values. While the other three products have relatively small mean bias values of about 0.04 m , UB_SIT has a large mean bias of about –0.14 m. UB_SIT performs well for ice thickness below 0.5 m but tends to underestimate ice thickness for thicker ice, which is consistent with the results of Sánchez-Gámez et al. (2020). Meanwhile, some points for UB_SIT in Fig. 8d are severely underestimated. The ULS ice thickness measurements range from 0.2 m to 0.6 m but the retrieved values of UB_SIT are close to 0 m, which may be explained by the fact that the UB_SIT assumes 100% sea ice concentration and the retrieved SIT will decrease when this condition is not fulfilled (Paţilea et al., 2019). In addition, UB_SIT relies on the brightness temperature for SIT estimation and the observed TB decreases with decreasing ice temperature which leads to underestimation of SIT under very cold conditions. By contrast, the utilization of PR(1.4) helps to eliminate the influence of physical ice temperature in SMOS_SIT and SMAP_SIT. It should be pointed out that among the four ice thickness products, SMOS_SIT and SMAP_SIT can obtain more data points for validation with the numbers being 1 416 and 977, respectively, inferring that these two algorithms can be applied to wider sea ice conditions. This may be attributed to the fact that SMOS_SIT and SMAP_SIT were trained on data from different years covering different regions of the Arctic.

4.5.2 *Validation using airborne sea ice thickness measurements*

The SIT products are further validated using airborne SIT measurements from two field campaigns of SafeWin 2011 and SMOSice 2014, which were conducted the northern Baltic Sea in March 2011 and in the Barents Sea in March 2014, respectively. Figure 9 shows the scatterplots between airborne SIT measurements and three SIT estimates (SMOS_SIT, UH_SIT and UB_SIT). It can be seen that SMOS_SIT has the best performance among the three products with bias and RMSE values being –0.10 m and 0.21 m, respectively. Although the SMOS_SIT retrieval algorithm was trained using the CFDD SIT obtained during the freezing period, SMOS_SIT is able to yield overall good results during the springtime. This may be associated with the representativeness of the training data since the CFDD SIT data were obtained from different years covering different regions of the Arctic. Both UH_SIT and UB_SIT underestimate the ice thickness with bias values being –0.27 m and –0.33 m, respectively, which agrees well with the results of Kaleschke et al. (2016).

5 Conclusions

This study developed an improved sea ice thickness SIT re-

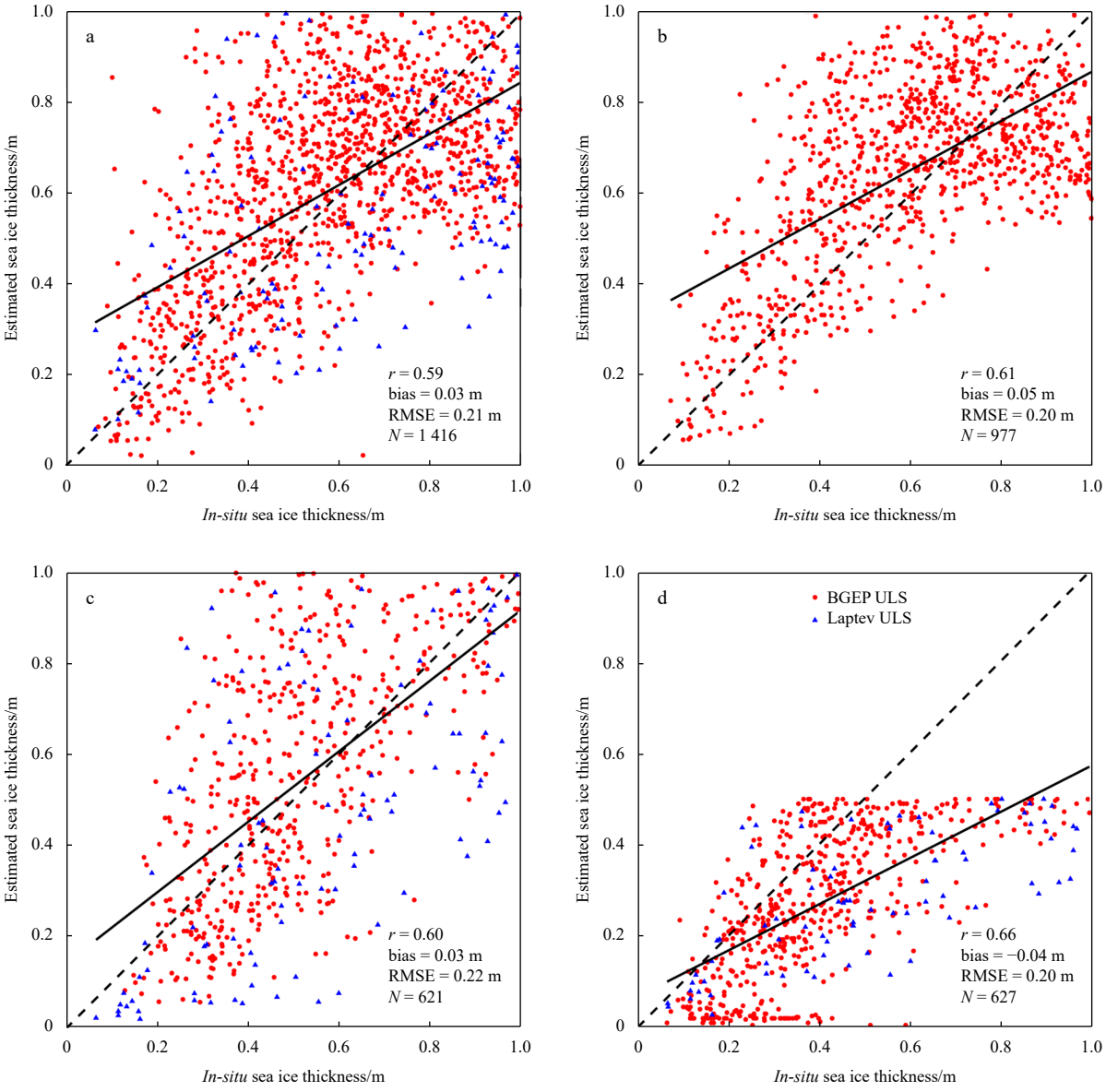

Fig. 8. Scatterplots between upward looking sonar sea ice thickness measurements and sea ice thickness retrievals for SMOS_SIT (a), SMAP_SIT (b), UH_SIT (c), and UB_SIT (d) during the cold seasons (October to January). Red dots represent data points from the Beaufort Sea for the period of 2010 to 2021 while blue triangles indicate data points from the Laptev Sea during the period of 2013 to 2015. Because the SMAP data are only available since March 2015, no data points are available in the Laptev Sea for SMAP_SIT. The black dash line indicates the 1:1 line while the black line indicated the fitted line. *r*, correlation coefficient.

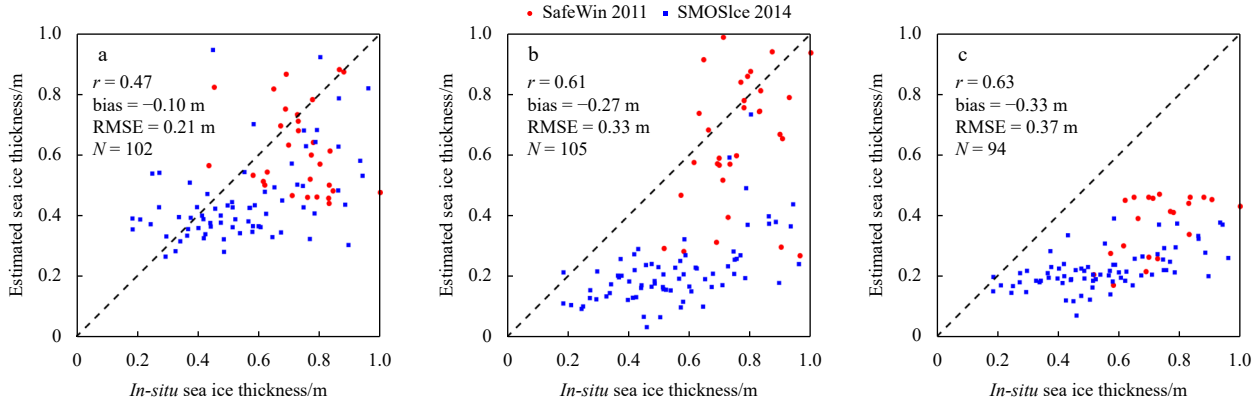

Fig. 9. Scatterplots between airborne sea ice thickness measurements and sea ice thickness retrievals for SMOS_SIT (a), UH_SIT (b), and UB_SIT (c) for campaigns of SafeWin 2011 and SMOSice 2014. The black dash line indicates the 1:1 line.

trieval algorithm for thin ice (< 1.0 m) in the Arctic Ocean from the SMAP and SMOS L-band brightness temperature observations during the freeze-up period. The improvements of the SIT retrieval algorithm include the correction for the sea ice concentration impact, reliable reference SIT data over different representative regions of the Arctic Ocean and the utilization of microwave polarization ratio that is independent of ice temperature. The accuracy of the proposed SIT retrieval algorithm was assessed using SIT measurements obtained from moored upward looking sonars and airborne electromagnetic induction sensors.

The cumulative freezing degree days model was applied over five carefully selected areas in the Beaufort, Chukchi, East Siberian, Laptev and Kara Seas during the freeze-up period to simulate thin ice thickness, which was further used as reference to study the relationship between SIT and the microwave polarization ratio of SMOS and SMAP at an incidence angle of 40°. The results show that the exponential function can well fit the relationship between PR and SIT and the regression coefficients are almost stable across the five selected regions, inferring that the proposed algorithm should be applicable to the entire Arctic Ocean.

The thin ice thickness products separately derived from SMOS and SMAP (i.e., SMOS_SIT and SMAP_SIT) in this study were compared with other products (i.e., UH_SIT from the University of Hamburg and UB_SIT from the University of Bremen) and then validated against SIT measurements from upward looking sonars in the Beaufort and Laptev seas and airborne electromagnetic induction sensors. The results indicate that SMOS_SIT and SMAP_SIT yield almost identical SIT retrievals and tend to achieve higher SIT values in the marginal ice zone compared to UH_SIT and UB_SIT due to the correction for the effect of sea ice concentration. When validating using ULS SIT data, SMOS_SIT and SMAP_SIT have comparable retrieval accuracy with UH_SIT and UB_SIT with RMSE values being about 0.20 m for the Beaufort Sea and 0.26 m for the Laptev Sea, respectively. When validating using EM SIT data, SMOS_SIT achieves the highest accuracy with RMSE being 0.21 m. The advantage of SMOS_SIT and SMAP_SIT over UH_SIT is the relative simplicity of the retrieval algorithm as well as less requirement for auxiliary data, while the advantage of SMOS_SIT and SMAP_SIT over UB_SIT is that PR(1.4) is independent of the physical ice temperature and can be used to operationally retrieve SIT up to 1.0 m.

The uncertainties in the retrieved SIT introduced by brightness temperature and sea ice concentration have been investigated using a Monte Carlo approach. The results indicate that the uncertainties in SIT retrievals introduced by radiometric uncertainties and sea ice concentration estimates increase with increasing SIT. SMOS has higher uncertainties than SMAP. The uncertainties introduced by sea ice concentration estimates are much less than that of radiometric uncertainties.

In this study, the snow layer on Arctic sea ice during the freeze-up period was assumed to dry and its radiative contribution on the sea ice brightness temperature can be neglected since dry snow is almost transparent at L-band (Maaß et al., 2013). However, the effect caused by snow layers on the relationship between PR and SIT warrants further analysis. Meanwhile, the performance of the proposed retrieval algorithm were validated using currently available ULS and EM SIT measurements. Due to the sparsity of *in situ* SIT measurements in the Arctic, it is important to assess the proposed retrieval algorithm over more periods and areas using other satellite SIT data such as SIT from thermal infrared data (Yu and Rothrock, 1996; Wang et al., 2010) in future studies.

References

Backus G E, Gilbert J F. 1967. Numerical applications of a formalism for geophysical inverse problems. Geophysical Journal International, 13(1–3): 247–276, doi: 10.1111/j.1365-246X.1967.tb02159.x

Belter H J, Janout M A, Krumpen T, et al. 2019. Daily mean sea ice draft from moored upward-looking sonars in the Laptev Sea between 2013 and 2015. PANGAEA, doi: 10.1594/PANGAEA.899275 [2019/2023-09-01]

Bilello M A. 1961. Formation, growth, and decay of sea-ice in the Canadian Arctic Archipelago. Arctic, 14(1): 2–24, doi: 10.14430/ARCTIC3658

Cavalieri D J. 1994. A microwave technique for mapping thin sea ice. Journal of Geophysical Research: Oceans, 99(C6): 12561–12572, doi: 10.1029/94JC00707

Chaubell J, Chan S, Dunbar R S, et al. 2020. SMAP enhanced L1C radiometer half-orbit 9 km EASE-Grid brightness temperatures, version 3. Boulder, Colorado, USA: NASA National Snow and Ice Data Center, doi: 10.5067/XB8K63YM4U8O, https://nsidc.org/data/spl1ctb_e/versions/3 [2021/2023-09-01]

Chi J, Kim H C. 2021. Retrieval of daily sea ice thickness from AMSR2 passive microwave data using ensemble convolutional neural networks. GIScience & Remote Sensing, 58(6): 812–830, doi: 10.1080/15481603.2021.1943213

Corbella I, Torres F, Duffo N, et al. 2011. MIRAS calibration and performance: results from the SMOS in-orbit commissioning phase. IEEE Transactions on Geoscience and Remote Sensing, 49(9): 3147–3155, doi: 10.1109/TGRS.2010.2102769

Entekhabi D, Njoku E G, O'Neill P E, et al. 2010. The Soil Moisture Active Passive (SMAP) mission. Proceedings of the IEEE, 98(5): 704–716, doi: 10.1109/JPROC.2010.2043918

Fukamachi Y, Simizu D, Ohshima K I, et al. 2017. Sea-ice thickness in the coastal northeastern Chukchi Sea from moored ice-profiling sonar. Journal of Glaciology, 63(241): 888–898, doi: 10.1017/jog.2017.56

Gupta M, Gabarro C, Turiel A, et al. 2019. On the retrieval of sea-ice thickness using SMOS polarization differences. Journal of Glaciology, 65(251): 481–493, doi: 10.1017/jog.2019.26

Haas C, Casey A, Lensu M. 2021. Safewin 2011 airborne EM sea ice thickness measurements in the Baltic Sea. PANGAEA, doi: 10.1594/PANGAEA.930545, https://doi.pangaea.de/10.1594/PANGAEA.930545 [2021/2023-09-01]

Hendricks S, Steinhage D, Helm V, et al. 2014. Final report: technical support for the 2014 SMOSice Campaign in SE Svalbard. Bremerhaven, Germany: Alfred Wegener Institute für Polar und Meeresforschung

Huntemann M, Heygster G, Kaleschke L, et al. 2014. Empirical sea ice thickness retrieval during the freeze-up period from SMOS high incident angle observations. The Cryosphere, 8(2): 439–451, doi: 10.5194/tc-8-439-2014

Ivanova N, Pedersen L T, Tonboe R T, et al. 2015. Inter-comparison and evaluation of sea ice algorithms: towards further identification of challenges and optimal approach using passive microwave observations. The Cryosphere, 9(5): 1797–1817, doi: 10.5194/tc-9-1797-2015

Iwamoto K, Ohshima K I, Tamura T, et al. 2013. Estimation of thin ice thickness from AMSR-E data in the Chukchi Sea. International Journal of Remote Sensing, 34(2): 468–489, doi: 10.1080/01431161.2012.712229

Kaleschke L, Lüpkes C, Vihma T, et al. 2001. SSM/I sea ice remote sensing for mesoscale ocean-atmosphere interaction analysis. Canadian Journal of Remote Sensing, 27(5): 526–537, doi: 10.1080/07038992.2001.10854892

Kaleschke L, Maaß N, Haas C, et al. 2010. A sea-ice thickness retrieval model for 1.4 GHz radiometry and application to airborne measurements over low salinity sea-ice. The Cryosphere, 4(4): 583–592, doi: 10.5194/tc-4-583-2010

Kaleschke L, Tian-Kunze X, Maaß N, et al. 2012. Sea ice thickness retrieval from SMOS brightness temperatures during the Arctic freeze-up period. Geophysical Research Letters, 39(5): L05501,

doi: 10.1029/2012GL050916
Kaleschke L, Tian-Kunze X, Maaß N, et al. 2016. SMOS sea ice product: operational application and validation in the Barents Sea marginal ice zone. Remote Sensing of Environment, 180: 264–273, doi: 10.1016/j.rse.2016.03.009
Kalnay E, Kanamitsu M, Kistler R, et al. 1996. The NCEP/NCAR 40-year reanalysis project. Bulletin of the American Meteorological Society, 77(3): 437–472, doi: 10.1175/1520-0477(1996)077<0437:TNYRP>2.0.CO;2
Kashiwase H, Ohshima K I, Fukamachi Y, et al. 2019. Evaluation of AMSR-E thin ice thickness algorithm from a mooring-based observation: how can the satellite observe a sea ice field with nonuniform thickness distribution?. Journal of Atmospheric and Oceanic Technology, 36(8): 1623–1641, doi: 10.1175/JTECH-D-18-0218.1
Kerr Y H, Waldteufel P, Wigneron J P, et al. 2001. Soil moisture retrieval from space: the Soil Moisture and Ocean Salinity (SMOS) mission. IEEE Transactions on Geoscience and Remote Sensing, 39(8): 1729–1735, doi: 10.1109/36.942551
Kim J M, Sohn B J, Lee S M, et al. 2020. Differences between ICESat and CryoSat-2 sea ice thicknesses over the Arctic: consequences for analyzing the ice volume trend. Journal of Geophysical Research: Atmospheres, 125(22): e2020JD033103, doi: 10.1029/2020JD033103
Kim J M, Sohn B J, Lee S M, et al. 2022. The estimation of the total freeboard of Arctic sea ice in winter using passive microwave satellite measurements. Journal of Atmospheric and Oceanic Technology, 39(10): 1611–1627, doi: 10.1175/JTECH-D-21-0105.1
Krishfield R, Proshutinsky A. 2006. BGOS ULS Data Processing Procedure. Woods Hole, MA, USA: Woods Hole Oceanographic Institute
Krishfield R A, Proshutinsky A, Tateyama K, et al. 2014. Deterioration of perennial sea ice in the Beaufort Gyre from 2003 to 2012 and its impact on the oceanic freshwater cycle. Journal of Geophysical Research: Oceans, 119(2): 1271–1305, doi: 10.1002/2013JC008999
Kwok R. 2018. Arctic sea ice thickness, volume, and multiyear ice coverage: losses and coupled variability (1958–2018). Environmental Research Letters, 13(10): 105005, doi: 10.1088/1748-9326/aae3ec
Kwok R, Cunningham G F. 2008. ICESat over Arctic sea ice: estimation of snow depth and ice thickness. Journal of Geophysical Research: Oceans, 113(C8): C08010, doi: 10.1029/2008JC004753
Lavergne T, Eastwood S, Teffah Z, et al. 2010. Sea ice motion from low-resolution satellite sensors: an alternative method and its validation in the Arctic. Journal of Geophysical Research: Oceans, 115(C10): C10032, doi: 10.1029/2009JC005958
Laxon S, Peacock N, Smith D. 2003. High interannual variability of sea ice thickness in the Arctic region. Nature, 425(6961): 947–950, doi: 10.1038/nature02050
Lee S M, Meier W N, Sohn B J, et al. 2021. Estimation of Arctic basin-scale sea ice thickness from satellite passive microwave measurements. IEEE Transactions on Geoscience and Remote Sensing, 59(7): 5841–5850, doi: 10.1109/TGRS.2020.3026949
Liu Yinghui, Key J R, Wang Xuanji, et al. 2020. Multidecadal Arctic sea ice thickness and volume derived from ice age. The Cryosphere, 14(4): 1325–1345, doi: 10.5194/tc-14-1325-2020
Maaß N, Kaleschke L, Tian-Kunze X, et al. 2013. Snow thickness retrieval over thick Arctic sea ice using SMOS satellite data. The Cryosphere, 7(6): 1971–1989, doi: 10.5194/tc-7-1971-2013
Mäkynen M, Similä M. 2019. Thin ice detection in the Barents and Kara Seas using AMSR2 high-frequency radiometer data. IEEE Transactions on Geoscience and Remote Sensing, 57(10): 7418–7437, doi: 10.1109/TGRS.2019.2913283
Mäkynen M, Similä M. 2022. AMSR2 thin ice detection algorithm for the Arctic winter conditions. IEEE Transactions on Geoscience and Remote Sensing, 60: 4303718, doi: 10.1109/TGRS.2022.3142966
Martin S, Drucker R, Kwok R, et al. 2004. Estimation of the thin ice thickness and heat flux for the Chukchi Sea Alaskan coast polynya from Special Sensor Microwave/Imager data, 1990–2001. Journal of Geophysical Research: Oceans, 109(C10): C10012, doi: 10.1029/2004JC002428
Martin S, Drucker R, Kwok R, et al. 2005. Improvements in the estimates of ice thickness and production in the Chukchi Sea polynyas derived from AMSR-E. Geophysical Research Letters, 32(5): L05505, doi: 10.1029/2004GL022013
Maslanik J, Stroeve J, Fowler C, et al. 2011. Distribution and trends in Arctic sea ice age through spring 2011. Geophysical Research Letters, 38(13): L13502, doi: 10.1029/2011GL047735
Maykut G A. 1978. Energy exchange over young sea ice in the central Arctic. Journal of Geophysical Research: Oceans, 83(C7): 3646–3658, doi: 10.1029/JC083iC07p03646
McMullan K D, Brown M A, Martin-Neira M, et al. 2008. SMOS: the payload. IEEE Transactions on Geoscience and Remote Sensing, 46(3): 594–605, doi: 10.1109/TGRS.2007.914809
Meier W N, Hovelsrud G K, van Oort B E H, et al. 2014. Arctic sea ice in transformation: a review of recent observed changes and impacts on biology and human activity. Reviews of Geophysics, 52(3): 185–217, doi: 10.1002/2013RG000431
Menashi J D, St Germain K M, Swift C T, et al. 1993. Low-frequency passive-microwave observations of sea ice in the Weddell Sea. Journal of Geophysical Research: Oceans, 98(C12): 22569–22577, doi: 10.1029/93JC02058
Naoki K, Ukita J, Nishio F, et al. 2008. Thin sea ice thickness as inferred from passive microwave and *in situ* observations. Journal of Geophysical Research: Oceans, 113(C2): C02S16, doi: 10.1029/2007JC004270
Paţilea C, Heygster G, Huntemann M, et al. 2019. Combined SMAP–SMOS thin sea ice thickness retrieval. The Cryosphere, 13(2): 675–691, doi: 10.5194/tc-13-675-2019
Peng Jinzheng, Misra S, Piepmeier J R, et al. 2019. Soil Moisture Active/Passive (SMAP) L-Band microwave radiometer post-launch calibration upgrade. IEEE Journal of Selected Topics in Applied Earth Observations and Remote Sensing, 12(6): 1647–1657, doi: 10.1109/JSTARS.2019.2902492
Petráš I, Bednárová D. 2010. Total least squares approach to modeling: a Matlab toolbox. Acta Montanistica Slovaca, 15(2): 158–170
Pfaffling A, Haas C, Reid J E. 2007. Direct helicopter EM—Sea-ice thickness inversion assessed with synthetic and field data. Geophysics, 72(4): F127–F137, doi: 10.1190/1.2732551
Piepmeier J R, Focardi P, Horgan K A, et al. 2017. SMAP L-Band microwave radiometer: instrument design and first year on orbit. IEEE Transactions on Geoscience and Remote Sensing, 55(4): 1954–1966, doi: 10.1109/TGRS.2016.2631978
Reid J E, Pfaffling A, Vrbancich J. 2006. Airborne electromagnetic footprints in 1D earths. Geophysics, 71(2): G63–G72, doi: 10.1190/1.2187756
Ricker R, Hendricks S, Kaleschke L, et al. 2017. A weekly Arctic sea-ice thickness data record from merged CryoSat-2 and SMOS satellite data. The Cryosphere, 11(4): 1607–1623, doi: 10.5194/tc-11-1607-2017
Sánchez-Gámez P, Gabarro C, Turiel A, et al. 2020. Assessment with controlled *in-situ* data of the dependence of L-Band radiometry on sea-ice thickness. Remote Sensing, 12(4): 650, doi: 10.3390/rs12040650
Scott K A, Buehner M, Carrieres T. 2014. An assessment of sea-ice thickness along the Labrador Coast from AMSR-E and MODIS data for operational data assimilation. IEEE Transactions on Geoscience and Remote Sensing, 52(5): 2726–2737, doi: 10.1109/TGRS.2013.2265091
Singh R K, Oza S R, Vyas N K, et al. 2011. Estimation of thin ice thickness from the Advanced Microwave Scanning Radiometer-EOS for coastal polynyas in the Chukchi and Beaufort Seas. IEEE Transactions on Geoscience and Remote Sensing, 49(8): 2993–2998, doi: 10.1109/TGRS.2011.2123101
Soriot C, Prigent C, Jimenez C, et al. 2023. Arctic sea ice thickness estimation from passive microwave satellite observations between 1.4 and 36 GHz. Earth and Space Science, 10(2): e2022EA002542, doi: 10.1029/2022EA002542

Spreen G, Kaleschke L, Heygster G. 2008. Sea ice remote sensing using AMSR-E 89-GHz channels. Journal of Geophysical Research: Oceans, 113(C2): C02S03, doi: 10.1029/2005JC003384

Tamura T, Ohshima K I. 2011. Mapping of sea ice production in the Arctic coastal polynyas. Journal of Geophysical Research: Oceans, 116(C7): C07030, doi: 10.1029/2010JC006586

Tian-Kunze X, Kaleschke L, Maaß N, et al. 2014. SMOS-derived thin sea ice thickness: algorithm baseline, product specifications and initial verification. The Cryosphere, 8(3): 997–1018, doi: 10.5194/tc-8-997-2014

Tietsche S, Alonso-Balmaseda M, Rosnay P, et al. 2018. Thin Arctic sea ice in L-band observations and an ocean reanalysis. The Cryosphere, 12(6): 2051–2072, doi: 10.5194/tc-12-2051-2018

Wang Xuanji, Key J R, Liu Yinghui. 2010. A thermodynamic model for estimating sea and lake ice thickness with optical satellite data. Journal of Geophysical Research: Oceans, 115(C12): C12035, doi: 10.1029/2009JC005857

Yoshizawa E, Shimada K, Cho K H. 2018. Algorithm for flat first-year ice draft using AMSR2 data in the Arctic Ocean. Journal of Atmospheric and Oceanic Technology, 35(11): 2147–2157, doi: 10.1175/JTECH-D-18-0034.1

Yu Youran, Rothrock D A. 1996. Thin ice thickness from satellite thermal imagery. Journal of Geophysical Research: Oceans, 101(C11): 25753–25766, doi: 10.1029/96JC02242